J Biomol NMR (2007) 38:11–22
DOI 10.1007/s10858-006-9131-9

ARTICLE

Joint composite-rotation adiabatic-sweep isotope filtration

Elizabeth R. Valentine · Fabien Ferrage · Francesca Massi · David Cowburn · Arthur G. Palmer III

Received: 10 October 2006 / Accepted: 29 November 2006 / Published online: 13 March 2007

Abstract Joint composite-rotation adiabatic-sweep isotope filters are derived by combining the composite-rotation [Stuart AC et al. (1999) J Am Chem Soc 121: 5346–5347] and adiabatic-sweep [Zwahlen C et al. (1997) J Am Chem Soc 119:6711–6721; Kupče E, Freeman R (1997) J Magn Reson 127:36–48] approaches. The joint isotope filters have improved broadband filtration performance, even for extreme values of the one-bond ^{1}H–^{13}C scalar coupling constants in proteins and RNA molecules. An average Hamiltonian analysis is used to describe evolution of the heteronuclear scalar coupling interaction during the adiabatic sweeps within the isotope filter sequences. The new isotope filter elements permit improved selective detection of NMR resonance signals originating from ^{1}H spins attached to an unlabeled natural abundance component of a complex in which the other components are labeled with ^{13}C and ^{15}N isotopes.

Keywords Composite pulse · J-filter · NOESY · Structure determination · vts SAM domain

E. R. Valentine · F. Massi · A. G. Palmer III (✉)
Department of Biochemistry and Molecular Biophysics, Columbia University, 630 West 168th Street, New York NY 10032, USA
e-mail: agp6@columbia.edu

F. Ferrage · D. Cowburn
New York Structural Biology Center, 89 Convent Avenue, New York, NY 10027-7556, USA

Present Address:
F. Ferrage
Département de Chimie, CNRS UMR 8642 École normale supérieure, 24 rue Lhomond, 75231 Paris Cedex 5, France

Introduction

Isotope-filtered and isotope-edited techniques are essential to the investigation of biological complexes by NMR spectroscopy (Otting and Wüthrich 1990). In these studies, one or a subset of the components of a complex are enriched in one or more NMR-active heteronuclei, for example ^{15}N or ^{13}C, and the other components are natural abundance or depleted in NMR-active isotopes. An isotope filter selectively suppresses and an isotope editor selectively detects resonance signals from ^{1}H spins directly attached to the NMR-active heteronuclei. These techniques rely on the differential evolution of ^{1}H spins subject to a large or small (near-zero) heteronuclear scalar coupling Hamiltonian. An alternative, more specific, nomenclature refers to an isotope filter as a low-pass *J*-filter and an isotope editor as a high-pass *J*-filter. Isotope filters are incorporated into NMR pulse sequences, such as COSY or TOCSY experiments, to permit resonance assignments of an unlabeled component of a complex and are incorporated into NOESY experiments to selectively detect NOE cross peaks between the ^{1}H spins within the unlabeled species or between the unlabeled and labeled components (Breeze 2000; Peterson et al. 2004).

The efficiency of isotope filters is reduced by variations in the one-bond scalar coupling constant between the ^{1}H spin and the heteronucleus. This difficulty is particularly severe for $^{1}H_n^{13}C$ (n = 1, 2, 3) moieties because J_{CH} depends on the nature of the chemical group, varying from ~120 Hz for CH_3 groups to ~220 Hz for the $^{1}H^{\varepsilon 1}$–$^{13}C^{\varepsilon 1}$ spin pair in histidine and the ^{1}H8–^{13}C8 spin pair in purine nucleotides. Two general approaches have emerged for improving the robustness

of low-pass *J*-filters despite variation in J_{CH}. The one approach relies on the isomorphism between pulse rotations and scalar coupling evolution (Levitt 1986). Composite pulses compensated for B_1 inhomogeneity are converted to sequence elements compensated for variation in J_{CH} (Stuart et al. 1999). The other approach uses the empirical relationship between the heteronuclear scalar coupling constant and isotropic ^{13}C chemical shift. Designed adiabatic broadband inversion pulses are used to effectively scale the coupling constants to a uniform value during an INEPT or other polarization transfer period (Kupče and Freeman 1997; Zwahlen et al. 1997).

In the present paper, the two approaches are combined to generate joint composite-rotation adiabatic-sweep isotope filter sequences, or low pass *J*-filters. The theoretical performance of the proposed sequences is evaluated using an average Hamiltonian description of the evolution of the heteronuclear scalar coupling interaction during an adiabatic sweep. The proposed sequences are validated using a ^{13}C-labeled Ala, Tyr, and His amino acid mixture, representing the range of J_{CH} encountered in proteins, and by recording a ^{1}H–^{1}H F1-filtered, F2-edited NOESY spectrum of the [U-^{13}C, U-^{15}N] Vts1 SAM domain complexed with its unlabeled cognate RNA ligand (Edwards et al. 2006).

Theory

Evolution of a spin system under the heteronuclear scalar coupling Hamiltonian during an adiabatic sweep has been treated theoretically by Kay and coworkers (Zwahlen et al. 1997, 1998). The adiabatic sweep is divided into a series of equal time intervals short enough that the amplitude and resonance offset of the rf field can be treated as constant during each interval. The evolution of the density matrix during the *i*th interval is calculated using as initial conditions the state of the density operator after the $(i-1)$th interval. Thus, evolution through the entire adiabatic sweep is calculated iteratively for the *N* intervals Δt_i for $i = 1,\ldots, N$, beginning with the initial conditions at the start of the adiabatic sweep. To simplify these calculations, Kay and coworkers developed compact expressions for efficiently calculating the evolution of a reduced set of basis operators during each interval.

In most applications, and in particular for isotope filtration, the state of the density operator does not need to be known at any arbitrary point within an adiabatic sweep; rather the net evolution of the density operator at the end of the sweep is of primary concern. In these circumstances, an average Hamiltonian theoretical treatment of evolution under the heteronuclear scalar coupling Hamiltonian is sufficiently accurate and yields simple intuitive results. Average Hamiltonian theory has been applied to adiabatic pulses for isolated spin systems, i.e. in the absence of scalar couplings, by Mitschang and Rinneberg (2003) and to homonuclear scalar coupled systems by Bennett et al. (2003).

The experimental situation of interest is illustrated in Fig. 1. The initial state of the density operator for an *I*–*S* spin system ($I = {}^{1}H$ and $S = {}^{13}C$) is described by an expansion in terms of in-phase (I_x and I_y) and antiphase transverse *I* spin product operators ($2I_xS_z$ and $2I_yS_z$). An adiabatic sweep of duration τ_p is applied to the *S* spin and a refocusing 180° is optionally applied to the *I*

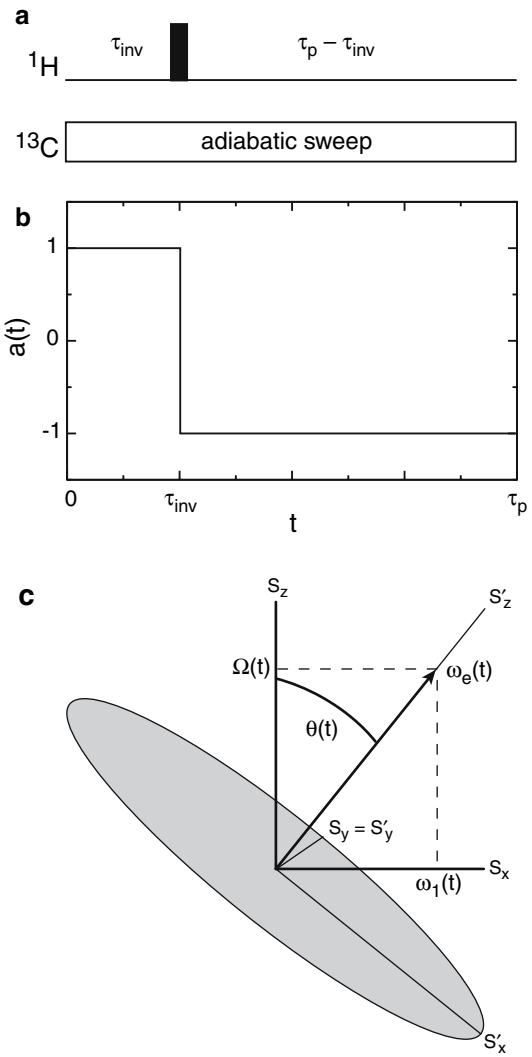

Fig. 1 Frequency-modulated interaction frame. (**a**) An adiabatic sweep is applied to the *S* spin while an 180° pulse is applied to the *I* spins at time t_{inv}. (**b**) The functional form of $a(t)$ is illustrated. (**c**) The tilted reference frame is shown schematically and the geometrical meanings of the main parameters are illustrated

spin at time τ_{inv}. The sequence element in Fig. 1a is formally equivalent to the sequence $-\tau_p$–[180°(I)] in which the Hamiltonian in the rotating frames of reference of the I and S spins during the period τ_p is given by

$$\mathcal{H}(t) = \Omega(t)S_z + \omega_1(t)S_x + a(t)2\pi J_{IS}I_zS_z \tag{1}$$

and the bracketed 180°(I) pulse is included only if a refocusing pulse is applied. The refocusing pulse inverts the scalar coupling interaction at time τ_{inv}; the effect of this pulse is represented by the function $a(t)$ with values

$$a(t) = \left\{ \begin{array}{cc} 1 & \text{when } 0 \le t \le \tau_{inv} \\ -1 & \text{when } \tau_{inv} < t \le \tau_p \\ 1 & \text{when no refocussing pulse is used} \end{array} \right\} \tag{2}$$

Without loss of generality, the I spin is assumed to be on-resonance in the rotating frame. The rotating frame of the S spin is defined relative to the instantaneous radiofrequency field of the adiabatic sweep, $\omega_{rf}(t)$; therefore, the frequency offset of the S spin is given by the time-dependent function $\Omega(t) = \omega_S - \omega_{rf}(t)$ and ω_S is the resonance frequency of the S spin. The amplitude of the adiabatic sweep, assumed to be applied with x-phase is given by $\omega_1(t)$. The amplitude and the tilt angle of the effective field in the rotating frame are given by $\omega_e(t) = [\Omega(t)^2 + \omega_1(t)^2]^{1/2}$ and $\tan[\theta(t)] = \omega_1(t)/\Omega(t)$, respectively. The time-variation of $\omega_e(t)$ and $\theta(t)$ are assumed to satisfy the adiabatic condition, in which the adiabaticity factor $Q = \omega_e/|d\theta(t)/dt| >> 1$; typically, the adiabaticity factor at resonance, $\Omega(t) = 0$, is chosen to satisfy $Q_0 > 5$.

Evolution under this Hamiltonian is analyzed most conveniently in a tilted frame of reference whose z'-axis is oriented along the instantaneous direction of $\omega_e(t)$. Transformation to the tilted frame is defined by $\hat{\mathcal{H}}(t) = U_1\mathcal{H}(t)U_1^{-1}$ with $U_1 = \exp[i\theta(t)S_y]$:

$$\begin{aligned}\hat{\mathcal{H}}(t) = {} & \omega_e(t)S'_z + a(t)2\pi J_{IS}\{I_zS'_z\cos[\theta(t)] \\ & - I_zS'_x\sin[\theta(t)]\}\end{aligned} \tag{3}$$

The propagator for evolution under this Hamiltonian can be written as (Haeberlen and Waugh 1968)

$$\mathbf{U}(t) = \mathbf{U}_0(t)\mathbf{U}_J(t) \tag{4}$$

in which

$$\mathbf{U}_0(t) = T\exp[-iS'_z\int_0^t \omega_e(t')dt'] \tag{5}$$

$$\mathbf{U}_J(t) = T\exp[-i\int_0^t \tilde{\mathcal{H}}(t')dt'] = \exp[i\bar{\mathcal{H}}] \tag{6}$$

T is the Dyson time-ordering operator (Evans and Powles 1967), and $\tilde{\mathcal{H}}(t)$ is the Hamiltonian expressed in the interaction frame rotating around the z' -axis with frequency $\omega_e(t)$. In this frame, illustrated in Fig. 1c, the Hamiltonian is given by:

$$\begin{aligned}\tilde{\mathcal{H}}(t) = {} & a(t)2\pi J_{IS}I_zS'_z\cos[\theta(t)] \\ & - a(t)\sin[\theta(t)]2\pi J_{IS}I_z\mathbf{U}_0(t)S'_x\mathbf{U}_0^{-1}(t) \\ = {} & a(t)2\pi J_{IS}I_zS'_z\cos[\theta(t)] - a(t)\sin[\theta(t)]2\pi J_{IS}I_z \\ & \{S'_x\cos[\omega_e(t)t] - S'_y\sin[\omega_e(t)t]\}\end{aligned} \tag{7}$$

The average Hamiltonian is

$$\bar{\mathcal{H}} = \bar{\mathcal{H}}^{(0)} + \bar{\mathcal{H}}^{(1)} + \ldots \tag{8}$$

in which

$$\bar{\mathcal{H}}^{(0)} = \frac{1}{t}\int_0^t \tilde{\mathcal{H}}(t_1)dt_1 \tag{9}$$

$$\bar{\mathcal{H}}^{(1)} = \frac{-i}{2t}\int_0^t dt_2\int_0^{t_2}[\tilde{\mathcal{H}}(t_2),\tilde{\mathcal{H}}(t_1)]dt_1 \tag{10}$$

In the applications envisioned, the transverse components of the interaction frame Hamiltonian given in Eq. 7, are negligible owing to rapid evolution of the sinusoidal terms that depend on $\omega_e(t)$. Thus, the zero-order average Hamiltonian is given by

$$\bar{\mathcal{H}}^{(0)} = \frac{1}{\tau_p}\int_0^{\tau_p} a(t')\cos[\theta(t')]dt'2\pi J_{IS}I_zS'_z = 2\pi\bar{J}_{IS}I_zS'_z \tag{11}$$

in which the reduced scalar coupling constant is defined by

$$\bar{J}_{IS} = \frac{J_{IS}}{\tau_p}\int_0^{\tau_p} a(t')\cos[\theta(t')]dt' \tag{12}$$

In the absence of a refocusing pulse:

$$\bar{J}_{IS} = \frac{J_{IS}}{\tau_p}\int_0^{\tau_p}\cos[\theta(t')]dt' = J_{IS} < \cos\theta > \tag{13}$$

in which angle brackets indicate the average value over the adiabatic sweep. If the average Hamiltonian can be truncated to its zeroth order (i.e. when the secular approximation can be applied to Eq. 7), the density operator in the laboratory frame at the end of the adiabatic sweep is given by:

$$\begin{aligned}\sigma(\tau_p) &= \exp[-i\theta(\tau_p)S_y]\mathbf{U}_0(\tau_p)\exp[-i\bar{\mathcal{H}}^{(0)}\tau_p]\sigma(0)\\ &\times \exp[i\bar{\mathcal{H}}^{(0)}\tau_p]\mathbf{U}_0^{-1}(\tau_p)\exp[i\theta(\tau_p)S_y]\\ &= \exp[-i\pi S_y]\exp[-i\bar{\mathcal{H}}^{(0)}\tau_p]\sigma(0)\\ &\quad \exp[i\bar{\mathcal{H}}^{(0)}\tau_p]\exp[i\pi S_y]\end{aligned} \tag{14}$$

The second equality is obtained because the propagator $\mathbf{U}_0(\tau_p)$ commutes with $\bar{\mathcal{H}}^{(0)}$ and the initial density operator and because the adiabatic sweep achieves a total rotation $\theta(\tau_p) = \pi$. Thus, evolution of the density operator during τ_p is obtained by the simple product operator rules for evolution under a reduced scalar coupling Hamiltonian $\bar{\mathcal{H}}^{(0)}$ followed by an ideal π S_y rotation; for example:

$$\begin{aligned}I_y &\xrightarrow{\tau_p} I_y\cos(\pi\bar{J}_{IS}\tau_p) + 2I_xS_z\sin(\pi\bar{J}_{IS}\tau_p)\\ 2I_xS_z &\xrightarrow{\tau_p} -2I_xS_z\cos(\pi\bar{J}_{IS}\tau_p) + I_y\sin(\pi\bar{J}_{IS}\tau_p)\end{aligned} \tag{15}$$

If a 180°(I) refocusing pulse is applied during the adiabatic sweep, then these results are modified by applying the 180°(I) pulse to the operators present after τ_p.

For a chirp pulse (Böhlen et al. 1990), a linear frequency sweep with a constant value of ω_1, Eq. 13 can be integrated to give

$$\begin{aligned}<\cos\theta> &= \frac{1}{2\Delta\Omega}\left\{\left[(\Delta\Omega+2\delta)^2+4\omega_1^2\right]^{1/2}\right.\\ &\quad \left.-\left[(\Delta\Omega-2\delta)^2+4\omega_1^2\right]^{1/2}\right\}\\ &\approx \frac{2\delta}{\Delta\Omega}\end{aligned} \tag{16}$$

in which $\Delta\Omega$ is the sweep bandwidth and δ is the frequency offset between the S spin and the center of the frequency sweep. The final approximation is obtained assuming that $\Delta\Omega^2 >> 2\omega_1^2 + 4\delta^2$. When this

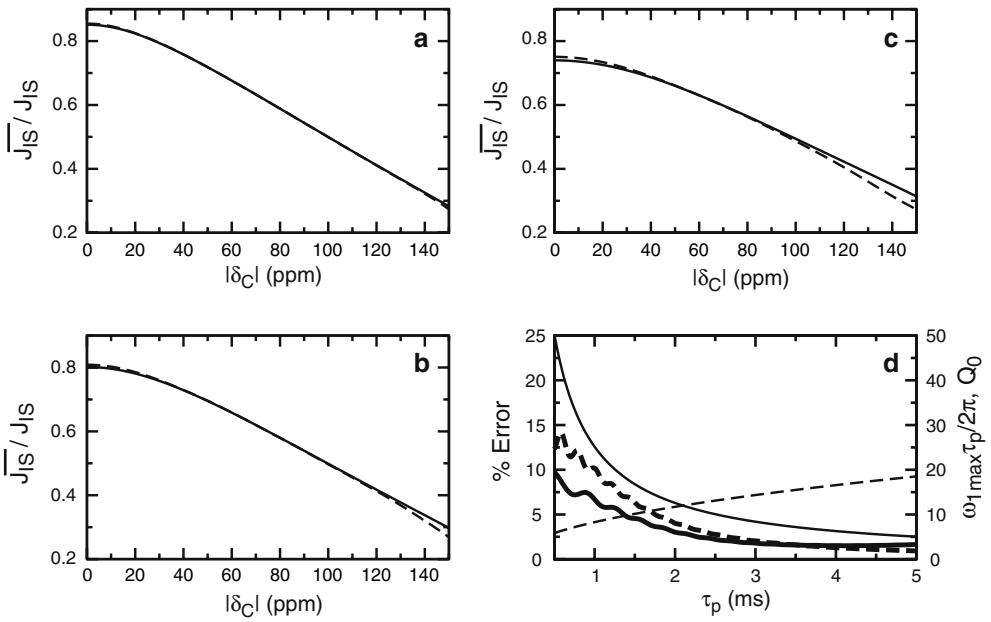

Fig. 2 Accuracy of average Hamiltonian theory. Results from average Hamiltonian theory calculated using Eq. 12 for the sequence element of Fig. 1a with $\tau_{inv} = \tau_p/2$ are compared to numerical calculations using the Liouville equation. The sweep used the WURST-20 shape (Kupče and Freeman 1995) with a sweep bandwidth $\Delta\Omega/2\pi = 60$ kHz (swept from –30 to +30 kHz) centered at a ^{13}C frequency of 0 ppm (for a 600 MHz NMR spectrometer). In (**a**) $\tau_p = 2.359$ ms, $\omega_{1max}/2\pi = 5$ kHz; (**b**) $\tau_p = 1.0$ ms, $\omega_{1max}/2\pi = 7$ kHz; (**c**) $\tau_p = 0.5$ ms, $\omega_{1max}/2\pi = 9.8$ kHz. The adiabaticity factors on-resonance at the center of the sweeps are Q_0 = (a) 6.65, (b) 5.13, and (c) 5.03 and the values of $\omega_{1max}\tau_p$ are (a) 74.1, (b) 44.0, and (c) 30.8. The solid line shows results for average Hamiltonian theory and the dashed line shows the exact numerical calculations. (**d**) The relative error $(\bar{J}_{IS}^{AHT} - \bar{J}_{IS}^{0})/\bar{J}_{IS}^{0}$, in which $\bar{J}_{IS}^{AHT}$ is calculated using using Eq. 12 and $\bar{J}_{IS}^{0}$ is calculated using the Liouville equation, is plotted for a ^{13}C spin 150 ppm off-resonance from the center of the adiabatic sweep, using a nominal value of $J_{IS} = 175$ Hz and $\Delta\Omega/2\pi = 60$ kHz (swept from –30 to +30 kHz). Shown are (dashed thick line) the percent error obtained when Q_0 is fixed at a value of 7.18 and (dashed thin line) $\omega_{1max}\tau_p/2\pi$ is varied and (solid thick line) the percent error obtained when $\omega_{1max}\ \tau_p/2\pi$ is fixed at a value of 15.5 and (solid thin line) Q_0 is varied

approximation is valid, evolution of the scalar coupling during an adiabatic sweep (in the absence of a refocusing 180° pulse applied to the I spins), can be represented as the sequence element τ' – 180° (S) – ($\tau_p - \tau'$), in which

$$\tau' = \frac{\tau_p}{2}\left(1 + \frac{2\delta}{\Delta\Omega}\right) \quad (17)$$

In Eq. 17, τ' is equal to the time at which the adiabatic frequency sweep is resonant with the S spin (Zwahlen et al. 1997). These results are approximately correct for the WURST family of adiabatic pulses (Kupče and Freeman 1995) as well, provided that δ is restricted to the central constant-amplitude region of the pulse.

The accuracy of the average Hamiltonian result of Eq. 12 is illustrated in Fig. 2 for the pulse sequence element of Fig. 1a using a series of WURST-20 adiabatic pulses (Kupče and Freeman 1995) with increasing field strengths and shorter durations, typical of values used for these pulses in biological NMR spectroscopy. As shown in Fig. 2d, the accuracy of the average Hamiltonian result is weakly dependent on the adiabaticity of the sweep, provided that adiabaticity is maintained ($Q_0 \geq 5$). Accuracy depends strongly on $\omega_{1max}\tau_p$, in which ω_{1max} is the peak value of $\omega_1(t)$ for three reasons. First, for large values of ω_{1max} and short values of τ_p, the quality factor can be smaller at the edges of the pulse (when the rf amplitude decays) than at its center. Although the error is negligible for a nuclear spin that is on-resonance at the center of the sweep (data not shown), Fig. 2d shows that the error can be relatively large for a spin inverted near the end of the sweep owing to violations of the adiabatic condition. This error can be reduced either by decreasing ω_{1max} or increasing the sweep bandwidth $\Delta\Omega$. Second, the accuracy of the approximation $\bar{\mathcal{H}} \approx \bar{\mathcal{H}}^{(0)}$, that is, keeping only the zero-order Hamiltonian in Eq. 8, requires that $\omega_{1max} >> \pi J_{IS}$. This condition is fulfilled over all ω_{1max} values in the calculations of Fig. 2d. Finally, the cosine and sine terms that depend on $\omega_e(t)t$ in Eq. 7 are averaged effectively to zero only if $\omega_{1max}\tau_p >> 1$. This condition is not satisfied for short values of τ_p, where the error shows an oscillatory behavior in Fig. 2d. Thus, the accuracy of the above results is reduced for either very weak rf fields, or short pulse lengths and narrow sweep bandwidths.

Rotations under on-resonance radiofrequency pulses in the operator space $\{I_x, I_y, I_z\}$ are isomorphous to rotations under the scalar coupling Hamiltonian in the operator space $\{2I_zS_z, 2I_xS_z, I_y\}$ (Levitt 1982). Thus, a composite 90° pulse that efficiently rotates I_z magnetization into the transverse plane independently of variation in the nominal rotational angle can be converted into a pulse-interrupted-free-precession period that transforms I_y magnetization efficiently into two-spin operators independently of variation in J_{IS}. The composite 90° pulse sandwich $\beta_0(2\beta)_{2\pi/3}$, in which the bracketed term is the nominal rotation angle and the subscript is the phase of the pulse, has previously been used by Stuart and coworkers to develop a highly efficient composite-rotation isotope filter (Stuart et al. 1999). Using the aforementioned isomorphism, the composite filter propagator is given by:

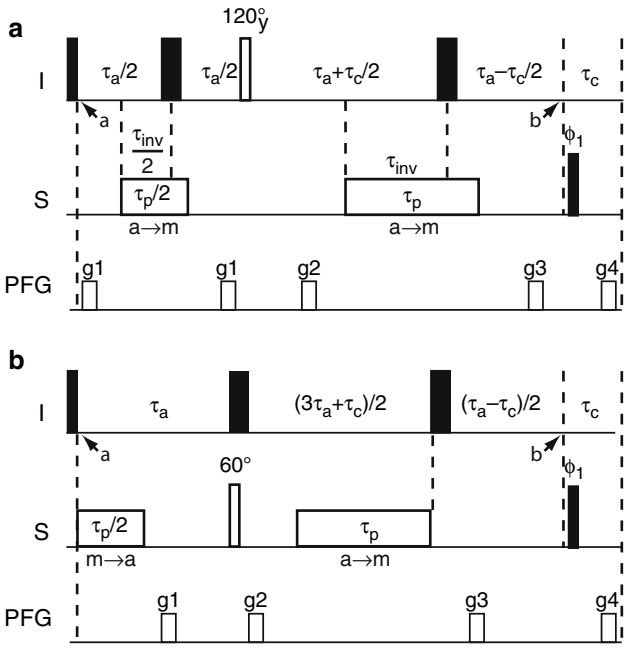

Fig. 3 Joint composite-rotation adiabatic-sweep isotope filters using (**a**) 120° I-spin rotation and (**b**) 60° S-spin rotation. Both filters are derived from the composite-rotation $\beta_0(2\beta)_{2\pi/3}$. Narrow and wide black bars represent 90° and 180° pulses, respectively; 180° pulses on the I spins can be applied as composite pulses. The narrow open bar represents an (**a**) 120° or (**b**) 60° pulse. Wide open bars applied at the ^{13}C frequency represent the two adiabatic sweeps. The direction of the frequency sweep is from low-to-high frequency (methyl-to-aromatic; m → a) or high-to-low frequency (aromatic-to-methyl; a → m) as indicated. The center of the frequency sweep is positioned at the center of the desired frequency range (~65 ppm for proteins and ~110 ppm for RNA). In (**a**), τ_{inv} is set so that the I-spin 180° pulse occurs when the instantaneous frequency is ~10 ppm upfield of the S-spin resonances (~0 ppm for proteins, ~50 ppm for RNA). All pulses have x-phase unless otherwise stated. Phase cycles are $\varphi_1 = x, -x$; and receiver phase = x. Gradients g1–g4 satisfy the relationships (a) $G_2\tau_2 = G_3\tau_3$ and (b) $G_1\tau_1 - G_2\tau_2 + G_3\tau_3 + G_4\tau_4 = 0$, in which G_k and τ_k are the gradient strength and duration of the kth gradient pulse. In (**a**) the value of τ_a is determined numerically; in (**b**), $\tau_a = 1/(2J_0) + \tau_p/2$. The delay τ_c is long enough to encompass the 90° pulse with phase φ_1 and the gradient g4

$$\begin{aligned}\mathbf{U} &= \exp[-i(2\beta)2I_{2\pi/3}S_z]\exp[-i\beta 2I_zS_z] \\ &= \exp[-i(2\beta)2\{I_z\cos(2\pi/3) + I_x \\ &\quad \sin(2\pi/3)\}S_z]\exp[-i\beta 2I_zS_z] \\ &= \exp[-i(2\pi/3)I_y]\exp[-i(2\beta)2I_zS_z] \\ &\quad \exp[i(2\pi/3)I_y]\exp[-i\beta 2I_zS_z]\end{aligned} \tag{18}$$

The leftmost I_y rotation is not needed to implement an isotope filter and can be eliminated to simplify the propagator to

$$\mathbf{U} = \exp[-i4\pi J_{IS}\tau I_zS_z]\exp[i(2\pi/3)I_y]\exp[-i2\pi J_{IS}\tau I_zS_z] \tag{19}$$

in which $\beta = \pi J_{IS}\tau$ and the filter is tuned to a nominal scalar coupling constant J_0 by setting the evolution delay $\tau = 1/(2J_0)$. This propagator is realized by the ideal filter pulse sequence:

$$\begin{aligned} I &: \frac{\tau}{2} - 180^\circ_x - \frac{\tau}{2} - 120^\circ_y - \tau - 180^\circ_x - \tau - \\ S &: \qquad 180^\circ_x \qquad\qquad 180^\circ_x \end{aligned} \tag{20}$$

A product operator analysis of the sequence shows that the evolution of I-spin coherence between points a and b of Fig. 3a is given by $-I_y \rightarrow -\varepsilon I_y$ in which:

$$\varepsilon = \cos^3[\pi J_{IS}\tau] \tag{21}$$

For a filter, the two-spin product operators created in this sequence, $2I_zS_z$ and $2I_xS_z$, are purged by a 90° pulse applied to the S spins. In other applications, optimal transfer to $2I_zS_z$ longitudinal two-spin order can be obtained by appending a final 30°_{-y} rotation to the sequence. For ^{1}H spins attached to ^{12}C nuclei, $J_{IS} = 0$ and $\varepsilon = 1$ under all conditions (ignoring relaxation).

As emphasized by Kay and coworkers (Zwahlen et al. 1997) and by Kupče and Freeman (1997), one-

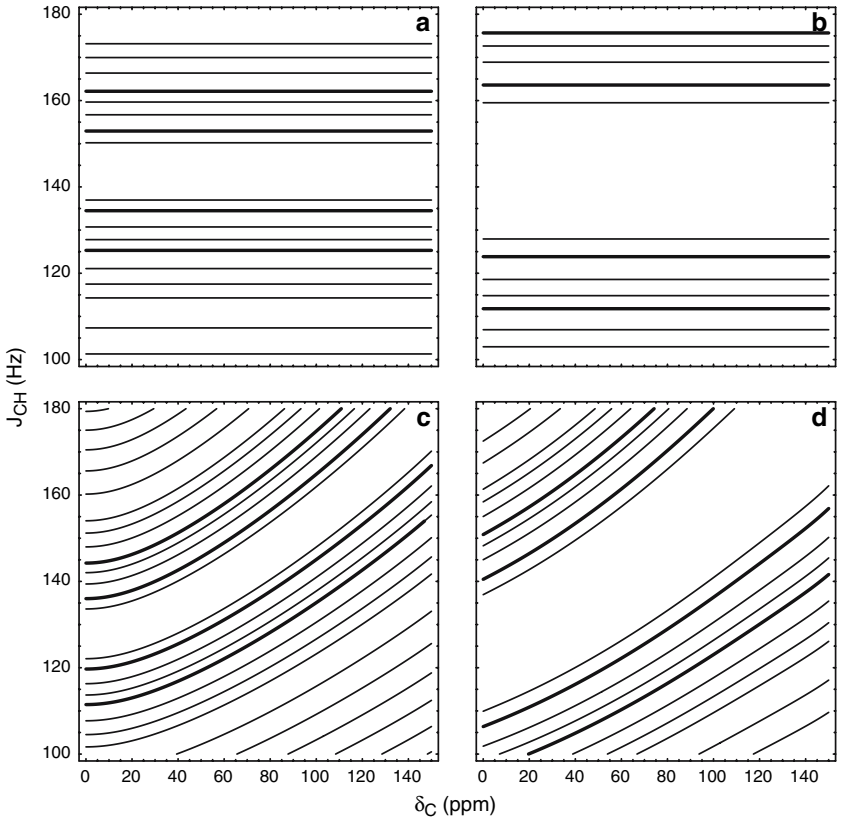

Fig. 4 Net I-spin coherence, ε, for isotope filters applied to proteins. (**a**) Second-order isotope filter with $\varepsilon = \cos^2[\pi J_{IS}/(2J_0)]$ and $J_0 = 144$ Hz. The filter is realized by setting $\tau_d = \tau_f = 1/(2J_0)$ and eliminating the pulse labeled "hg" in Fig. 3b of Kay and coworkers (Zwahlen et al. 1997). (**b**) Isotope filter derived from a $\beta_0(2\beta)_{2\pi/3}$ composite rotation with $\varepsilon = \cos^3[\pi J_{IS}/(2J_0)]$ and $J_0 = 144$ Hz (Stuart et al. 1999). (**c**) Adiabatic sweep filter taken from Fig. 3c of Kay and coworkers (Zwahlen et al. 1997). Calculations used $\tau_a = 2.1$ ms, and the WURST-20 adiabatic sweep (Kupče and Freeman 1995) centered at 0 ppm with $\tau_p = 1.944$ ms, $\Delta\Omega/2\pi = 60$ kHz and $\omega_{1max}/2\pi = 5$ kHz. (**d**) Joint composite-rotation adiabatic-sweep isotope filter of Fig. 3b with ε given by Eq. 25. Calculations used $\tau_a = 4.48$ ms and the WURST-20 adiabatic sweep (Kupče and Freeman 1995) centered at 65 ppm with $\tau_p = 2.0$ ms, $\Delta\Omega/2\pi = 30$ kHz and $\omega_{1max}/2\pi = 5$ kHz. Contour lines are drawn at ε = {0.005, 0.01, 0.02, 0.03, 0.04, 0.06, 0.08, 0.10, 0.15, 0.20, 0.25, 0.30, 0.35, 0.40}. Heavier lines are drawn for ε = {0.01, 0.04}

bond C–H scalar coupling constants and isotropic chemical shifts are linearly related for ^{1}H spins attached to ^{13}C nuclei in amino acid residues and RNA nucleotides:

$$J_{\mathrm{IS}} \approx 120 + 0.365\delta_C \qquad \text{(amino acids)} \qquad (22)$$

$$J_{\mathrm{IS}} \approx 101 + 0.710\delta_C \qquad \text{(RNA)} \qquad (23)$$

in which J_{IS} is measured in Hz and δ_C is the chemical shift measured in ppm (relative to DSS). As shown by Eq. 12, the reduced scalar coupling constant during an adiabatic sweep also depends on the *S*-spin resonance offset. Accordingly, the pulse element shown in Fig. 1a can be substituted for the central pair of 180° pulses in an INEPT element. The properties of the adiabatic sweep are chosen to obtain broadband polarization transfer from initial $-I_y$ magnetization to $2I_xS_z$ for the desired range of J_{IS}. This strategy has been elegantly incorporated into double-tuned isotope filters by Kay and coworkers (Zwahlen et al. 1997).

Two implementations of a joint composite-rotation adiabatic-sweep filter element are shown in Fig. 3. The two filter sequences have essentially the same theoretical performance. In the sequence of Fig. 3a, the two adiabatic pulses have the same frequency bandwidth and are swept in the same sense; therefore, the values of $\bar{J}_{\mathrm{IS}}$ calculated using Eq. 12 are identical for the two adiabatic sweeps. A product operator analysis of the sequence shows that the evolution of *I*-spin coherence between points *a* and *b* of Fig. 3a is given by $-I_y \rightarrow -\varepsilon I_y$ in which:

$$\varepsilon = \cos^3\left[\frac{1}{2}\pi J_{\mathrm{IS}}\{2\tau_a - \tau_{\mathrm{p}}(1 - \bar{J}_{\mathrm{IS}}/J_{\mathrm{IS}})\}\right] \qquad (24)$$

In the sequence of Fig. 3b, the second adiabatic pulse, of length τ_{p}, has the same sweep bandwidth, but is swept in the opposite sense as the first adiabatic sweep. Therefore $<\cos[\theta(t)]>_{\mathrm{sweep2}} = -<\cos[\theta(t)]>_{\mathrm{sweep1}} = <\cos\theta>$ using Eq. 13. A product operator analysis of the sequence shows that the evolution of *I*-spin coherence between points *a* and *b* of Fig. 3b is given by $-I_y \rightarrow -\varepsilon I_y$in which:

$$\varepsilon = \cos^3\left[\frac{1}{2}\pi J_{\mathrm{IS}}\{2\tau_{\mathrm{a}} - \tau_{\mathrm{p}}(1 - <\cos\theta>)\}\right] \qquad (25)$$

The filters are implemented by numerically optimizing the adiabatic sweeps in order to minimize ε in Eqs. 24 and 25 over the desired range of J_{IS} (while maintaining adiabaticity of the sweep as a constraint). For ^{1}H spins attached to ^{12}C nuclei, $J_{\mathrm{IS}} = 0$ and $\varepsilon = 1$ under all conditions (ignoring relaxation). Figure 4 compares the theoretical performance of the joint composite-rotation adiabatic-sweep isotope filter for scalar coupling constants in proteins with other approaches that have been described in the literature. The corresponding theoretical performance for scalar coupling constants in RNA is shown in Fig. 5. The improvements obtained with the new sequences, particularly at the low and high extremes of the scalar coupling constants, are evident. The sequence of Fig. 3a is derived from the basic composite rotation $\beta_0(2\beta)_{2\pi/3}$ in a more straightforward fashion; however, as discussed below, the sequence of Fig. 3b has only 180° pulses on the *I*-spin when transverse coherences are present and allows convenient water suppression with the excitation sculpting (Hwang and Shaka 1995) approach. In addition, resonance offset effects are smaller for a 60° pulse compared with a 120° pulse.

The above theoretical analyses do not include the effects of relaxation. The joint composite-rotation adiabatic-sweep isotope filters are longer than the corresponding composite-rotation sequences of Stuart et al. (1999), for example, the sequence of Fig. 3b is longer by $3\tau_{\mathrm{p}}/2$, leading to reduced sensitivity, owing to relaxation losses. Thus, the lengths of the adiabatic sweeps also should be minimized while satisfying Eqs. 24 and 25. Transverse relaxation for ^{1}H spins attached to ^{13}C nuclei is more efficient than for ^{1}H spins attached to ^{12}C nuclei, because the ^{1}H–^{13}C dipolar interaction constitutes an additional relaxation mechanism. Consequently, the apparent filter efficiency,

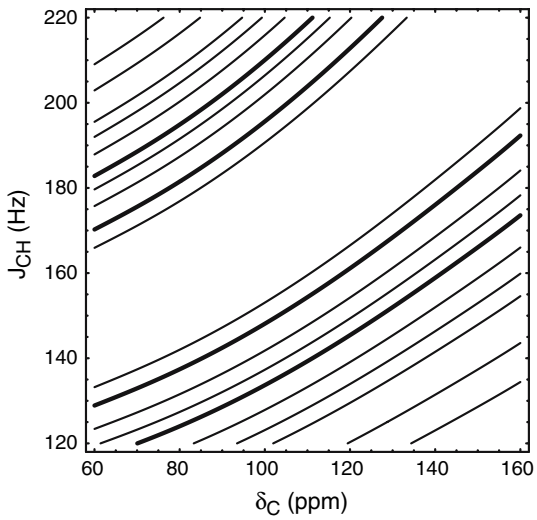

Fig. 5 Net *I*-spin coherence, ε, for isotope filtration in RNA. Joint composite-rotation adiabatic-sweep isotope filter of Fig. 3b with ε given by Eq. 25. Calculations used $\tau_{\mathrm{a}} = 3.69$ ms and the WURST-20 adiabatic sweep (Kupče and Freeman 1995) centered at 110 ppm with $\tau_{\mathrm{p}} = 1.8$ ms, $\Delta\Omega/2\pi = 20$ kHz and $\omega_{1\mathrm{max}}/2\pi = 4.5$ kHz. Contour lines are drawn at ε = {0.005, 0.01, 0.02, 0.03, 0.04, 0.06, 0.08, 0.10, 0.15, 0.20, 0.25, 0.30, 0.35, 0.40}. Heavier lines are drawn for ε = {0.01, 0.04}

measured as the ratio of peak intensities for ^{1}H spins attached to ^{12}C nuclei and for ^{1}H spins attached to ^{13}C nuclei is increased in larger proteins with larger transverse relaxation rate constants.

Methods

The new isotope filter elements can be used as building blocks in a number of different pulse sequences as shown in Figs. 6 and 7. Figure 6a shows an F1/F2-edited, F3-filtered HMQC-NOESY experiments based on a semi-constant-time HMQC pulse sequence. The excitation sculpting water suppression technique (Hwang and Shaka 1995) has been built into the filter element, without increase in any delays, for water suppression. Figure 6b shows an F1-filtered, F2/F3-edited NOESY-HMQC pulse sequence. The excitation sculpting technique has been built into the HMQC pulse sequence for water suppression. Both of these sequences use phase cycling for ^{13}C editing and subtraction artifacts may pose a significant problem if large excesses of unlabeled

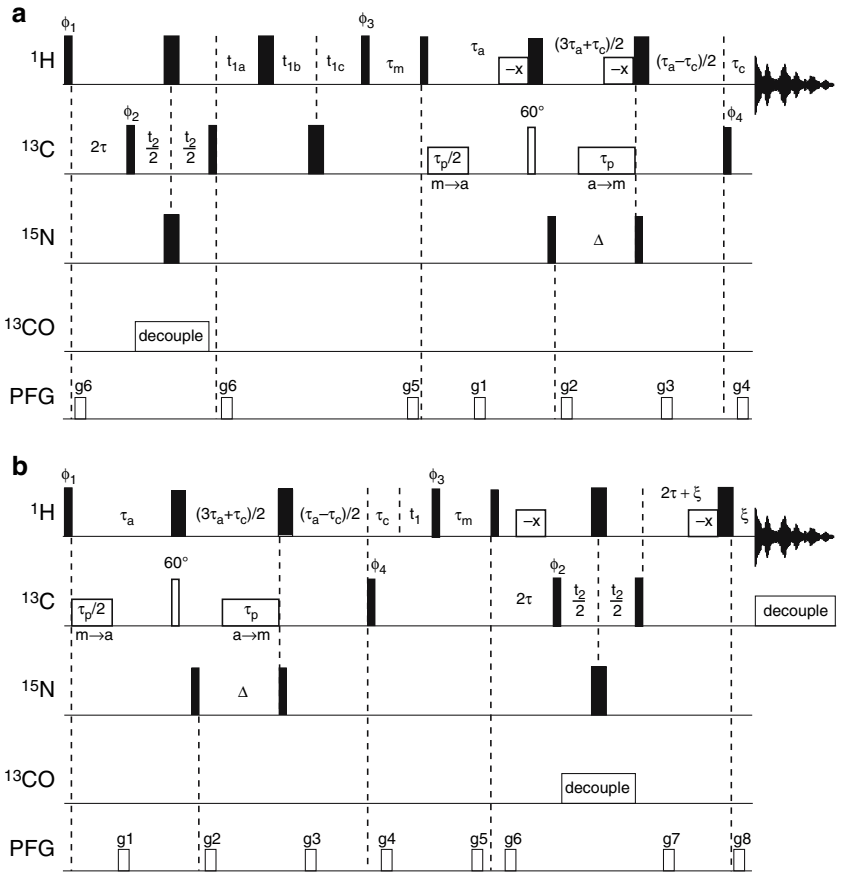

Fig. 6 (**a**) F1/F2-edited, F3-filtered HMQC-NOESY and (**b**) F1-filtered, F2/F3-edited NOESY-HMQC pulse sequences. Narrow and wide black bars represent 90° and 180° pulses, respectively. The narrow open bar represents a 60° pulse. Wide open bars applied at the ^{13}C frequency represent the two adiabatic sweeps; open bars applied at the ^{1}H frequency represent water selective rectangular 180° pulses. All pulses have x-phase unless otherwise stated. Phase cycles are $\varphi_1 = x, -x$; $\varphi_2 = x, x, -x, -x$; $\varphi_3 = 8(x), 8(-x)$; $\varphi_4 = 4(x), 4(-x)$; $\varphi_5 = x$; and receiver phase $= x, -x, -x, x, -x, x, x, -x$. Gradients g1–g4 satisfy the relationships $G_1\tau_1 - G_2\tau_2 + G_3\tau_3 + G_4\tau_4 = 0$, in which G_k and τ_k are the gradient strength and duration of the kth gradient pulse. In (**a**), these gradients also achieve excitation sculpting water suppression (Hwang and Shaka 1995); in (**b**), water suppression uses gradients g6, g7, and g8, satisfying $G_6\tau_6 - G_7\tau_7 + G_8\tau_8 = 0$. Other gradients are for artifact suppression. Quadrature detection in t_1 and t_2 is achieved by the TPPI-States method (Marion et al. 1989). (a) Semi-constant-time frequency labeling (Grzesiek and Bax 1993; Logan et al. 1993) is used for t_1 by variation of t_{1a}, t_{1b}, and t_{1c}. The initial values of these delays are $t_{1a}(0) = 2\tau$ and $t_{1b}(0) = t_{1c}(0) = 0$. The value of t_{1a} is decremented by Δt_{1a} and t_{1b}, and t_{1c} are incremented by Δt_{1b} and Δt_{1c}, respectively. These values are chosen to satisfy the requirement that the minimum value of t_{1a} must be greater than the duration of g4, $1/SW_1 = \Delta t_{1a} + \Delta t_{1b} + \Delta t_{1c}$, and $\Delta t_{1a} - \Delta t_{1b} + \Delta t_{1c} = 0$, in which SW1 is the spectral width in the t_1 dimension. Decoupling of ^{13}CO spins is accomplished using SEDUCE-1 (McCoy and Mueller 1993). Decoupling during acquisition uses GARP (Shaka et al. 1985) (or an adiabatic decoupling procedure). Parameters for the filter element are described in the caption to Fig. 3b. Other delays are $\Delta = 5.4$ ms for isotope filtration of ^{15}N-attached ^{1}H spins, $2\tau = 3.47$ ms, and ξ is longer than the duration of g8

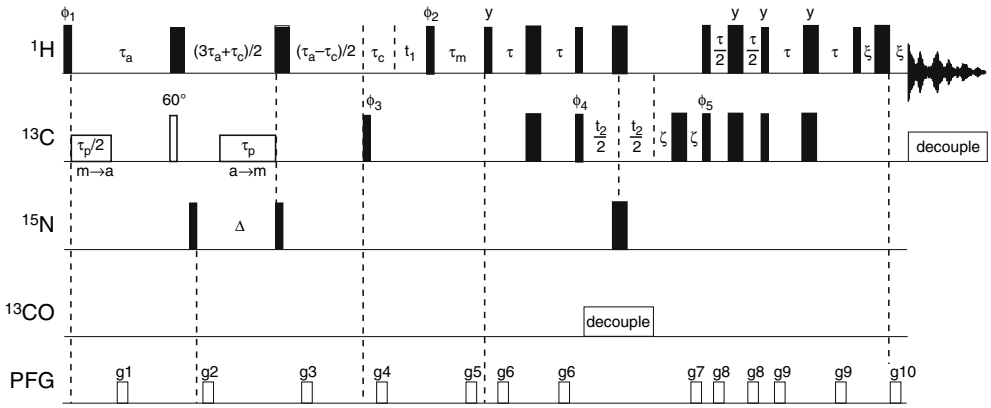

Fig. 7 F1-filtered, F2/F3-edited NOESY-HSQC isotope filtered pulse sequence. Narrow and wide black bars represent 90° and 180° pulses, respectively. The narrow open bar is a 60° pulse. Wide open bars are the two adiabatic sweeps. All pulses have *x*-phase unless otherwise stated. Phase cycles are $\varphi_1 = x, -x$; $\varphi_2 = x, x, -x, -x$; $\varphi_3 = 8(x), 8(-x)$; $\varphi_4 = 4(x), 4(-x)$; $\varphi_5 = x$; and receiver phase = $x, -x, -x, x, -x, x, x, -x$. Gradients g1–g4 satisfy the relationships $G_1\tau_1 - G_2\tau_2 + G_3\tau_3 + G_4\tau_4 = 0$, in which G_k and τ_k are the gradient strength and duration of the *k*th gradient pulse. Gradients g7 and g10 are used for gradient coherence selection; other gradients are for artifact suppression. Quadrature detection in t_1 is achieved by the TPPI-States method (Marion et al. 1989); echo-antiecho quadrature detection in t_2 is achieved by inverting φ_5 and the sign of gradient g7 (Kay et al. 1992); axial peaks are shifted by inverting φ_1, and the receiver phase. Decoupling during t_2 and t_3 use the SEDUCE-1 (McCoy and Mueller 1993) and GARP (Shaka et al. 1985) (or an adiabatic decoupling procedure), respectively. Parameters for the filter element are described in the caption to Fig. 3b. Other delays are $\Delta = 5.4$ ms for isotope filtration of ^{15}N-attached ^{1}H spins, $\tau = 3.47$ ms, ζ is longer than the duration of g7, and ξ is longer than the duration of g10

ligands (or buffer components) are present in the sample; however, the HMQC-NOESY sequence in particular has the advantage for use with cryogenic probes of not requiring decoupling during acquisition. Figure 7 shows a F1-filtered, F2/F3-edited NOESY-HSQC pulse sequence that uses the gradient-selected sensitivity-enhanced pulse sequence element (Kay et al. 1992; Palmer et al. 1991; Schleucher et al. 1994) for improved ^{13}C editing.

The accuracy of the average Hamiltonian treatment of adiabatic sweeps and the performance of the proposed composite-rotation adiabatic-sweep isotope filter elements were validated using a sample containing [99%-^{13}C]-labeled Ala, His, and Tyr amino acids (~1 mM in 100% D_2O) (Cambridge Isotopes). The reduced scalar coupling constant for the Ala $^1H^\alpha$ resonance was measured as a function of resonance offset using the pulse sequence in the inset to Fig. 8b. The performance of the proposed filter was measured using the sequence in Fig. 3b by recording a single-transient free-induction decay immediately following the filter sequence (i.e., no additional isotope-editing was performed after the filter). Weak presaturation was used prior to the first pulse for water suppression. A ^{1}H–^{1}H F1-filtered, F2-edited NOESY spectrum was recorded using a 0.5 mM sample of a 1:1 complex between [U-^{13}C, U-^{15}N] Vts1 SAM domain and natural abundance TCE 13mer RNA (10% D_2O/90% H_2O, pH = 6.25) described elsewhere (Edwards et al. 2006). The spectrum was recorded using the pulse sequence of Fig. 7 by setting $t_2 = 0$. The spectrum was recorded in ~18 h using (F1 × F2) spectral widths of (6,250 Hz × 12,500 Hz) as a (175 × 1024) complex matrix. A total of 128 scans were recorded per complex t_1 point. The NOE mixing time was 250 ms. All experiments were recorded using a Bruker DRX600 NMR spectrometer equipped with a cryogenic triple resonance probe with a *z*-axis gradient.

Results

Figure 8 illustrates the application of average Hamiltonian theory for treating scalar coupling interactions during adiabatic sweeps. Figure 8a shows the instantaneous values of $\cos[\theta(t)]$ during an adiabatic sweep for three different values of the resonance offset. During the adiabatic sweep, the value of $\cos[\theta(t)]$ is null when the rf field is resonant with the nuclear spin. The value of $<\cos\theta>$ is given by the integral of the curves and is equal to zero only for a spin resonant with the rf field at the center of the sweep. Figure 8b shows the reduced scalar coupling constant measured for the Ala $^1H^\alpha$ resonance as a function of resonance offset from the value of the rf field at the center of the sweep for the spin-echo pulse sequence shown in the inset. Measured values of the reduced coupling constant are shown as solid circles. The line is not a fit to the data; rather, the line is calculated using average Hamiltonian theory and independently determined

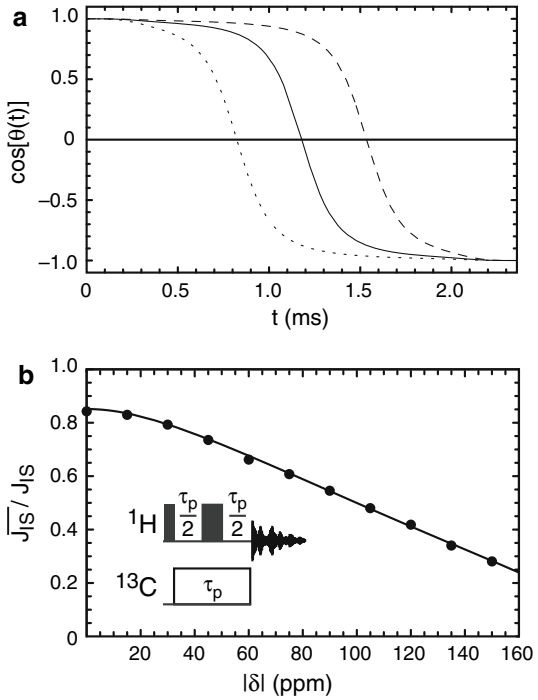

Fig. 8 *J*-scaling during adiabatic sweep. (**a**) Plots of $\cos[\theta(t)]$ versus t during an adiabatic sweep. The sweep used the WURST-20 shape (Kupče and Freeman 1995) with τ_p = 2.359 ms, a sweep bandwidth $\Delta\Omega/2\pi$ = 60 kHz (swept from –30 to +30 kHz), and $\omega_{1max}/2\pi$ = 5 kHz. The solid line shows results for a spin on-resonance with the center of the sweep (δ = 0); the dotted (dashed) line shows results for a spin with resonance offset $\delta/2\pi$ = –9 kHz (+9 kHz). Values of $< \cos\theta >$ = $(3.2 \times 10^{-5})\Omega$ are linear over the range $\delta/2\pi$ = –20 to +20 kHz as obtained using Eq. 13. (**b**) Experimental validation of the average Hamiltonian expression for the reduced scalar coupling constant. The scalar coupling constant for the Ala $^1H^{\alpha}$ resonance was measured as a function of offset from the center of the adiabatic sweep on a 600 MHz NMR spectrometer using the pulse sequence shown in the inset. The adiabatic sweep used the same parameters as in (**a**). The points give the experimental result and the line gives the calculated (not fitted) values obtained from Eq. 12.

parameters used for the adiabatic sweep in the pulse sequence element.

Figure 9 shows the degree of suppression achieved by the joint composite-rotation adiabatic-sweep filter in a single scan using the pulse sequence of Fig. 3b (nearly identical results are obtained using the pulse sequence of Fig. 3a). The residual filter breakthrough peaks, even for the His $^1H^{\varepsilon 1}$ resonances (8.28 and 8.66 ppm) and Ala $^1H^{\beta}$ resonances (1.26 and 1.50 ppm) are < 0.01 (smaller than the centerband resonance peaks for ^{1}H spins attached to ^{12}C nuclei, resulting from the ~1% of carbon sites that are not isotopically enriched in the 99% labeled amino acids). Improvements compared with the individual composite-rotation isotope filter

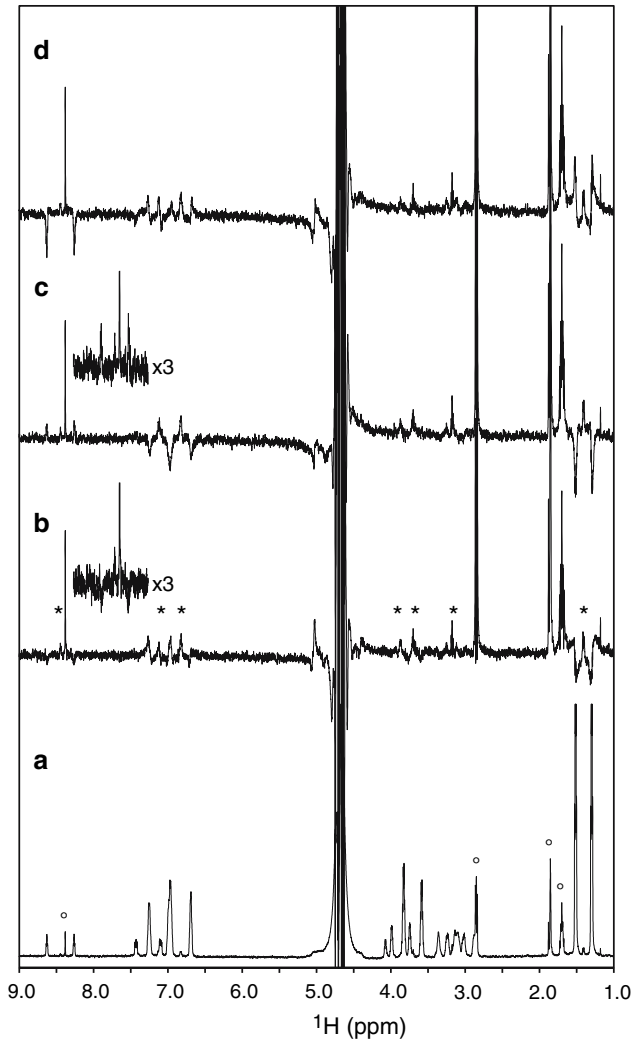

Fig. 9 Isotope filtration efficiency. A sample containing [U-^{13}C] Ala, [U-^{13}C] Tyr, and [U-^{13}C] His amino acids was used to test the isotope filtration performance in a single (one-scan) transient. (**a**) One-pulse ^{1}H NMR spectrum; (**b**) isotope filtered ^{1}H NMR spectrum using the filter of Fig. 3b; (**c**) isotope-filtered ^{1}H NMR spectrum using the filter taken from Fig. 3c of Kay and coworkers (Zwahlen et al. 1997); (**d**) isotope-filtered ^{1}H NMR spectrum using in the filter described by Stuart and coworkers (Stuart et al. 1999). In (b) τ_a = 4.608 ms, and the WURST-20 adiabatic sweep (Kupče and Freeman 1995) was centered at 68 ppm with τ_p = 2.115 ms, $\Delta\Omega/2\pi$ = 32.5 kHz and $\omega_{1max}/2\pi$ = 5 kHz. Gradients had the shape of the center lobe of a sine function and a length of 500 μs. Gradient amplitudes were $G1$ = 11 G/cm, $G2$ = 26 G/cm, $G3$ = –15 G/cm, and $G4$ = 30 G/cm. In (**c**) τ_a = 2.1 ms, and the WURST-20 adiabatic sweeps (Kupče and Freeman 1995) were centered at 0 ppm with τ_p = 1.944 ms, $\Delta\Omega/2\pi$ = 60 kHz and $\omega_{1max}/2\pi$ = 5 kHz. The spectrum in (a) is scaled by a factor 0.2. The insets in (**b**) and (**c**) shown the region from 8 to 9 ppm expanded vertically by a factor of 3 to better show the His $^1H^{\varepsilon 1}$ resonances at 8.28 and 8.66 ppm. Resonance peaks for ^{1}H spins attached to ^{12}C nuclei, resulting from the ~1% of carbon sites that are not isotopically enriched, are labeled with "*" in (**b**). Buffer contaminants are labeled with "°" in (**a**)

and the adiabatic-sweep isotope filter are particularly evident for the His $^{1}H^{\varepsilon 1}$ resonances.

Figure 10 displays the region of the ^{1}H-^{1}H F1-filtered, F2-edited NOESY spectrum corresponding to the F1 RNA sugar region and F2 protein methyl region. A number of RNA-protein crosspeaks are visible (along with a ridge of water-to-protein NOE crosspeaks). The residual diagonal resonances, resulting from filter breakthrough, are inverted and approximately are of the same intensity as the stronger NOE crosspeaks.

Discussion and conclusion

Two distinct approaches for improving the performance of isotope filters, one based on composite-rotations (Stuart et al. 1999) and the other based on designed adiabatic sweeps (Kupče and Freeman 1997; Zwahlen et al. 1997), have been reported previously. Combination of the two approaches yields superior filtration efficiency, compared with methods individually, particularly for ^{1}H spins with coupling constants that are near the extrema of the range of values or that do not satisfy empirical relationships between isotropic chemical shifts and scalar coupling constants. The latter property makes the new filter sequences particularly useful for molecular complexes that are weakly aligned in anisotropic media (Tjandra and Bax 1997). In such samples, the residual heteronuclear dipole coupling adds to the heteronuclear scalar coupling constant and renders the approximate relationships between scalar coupling constants and isotropic shifts in Eqs. 22 and 23 less accurate. The joint composite-rotation adiabatic-sweep isotope filter can be incorporated as a building block in a variety of NMR pulse sequences to obtain NMR spectra that are isotope-filtered in one or more frequency domains.

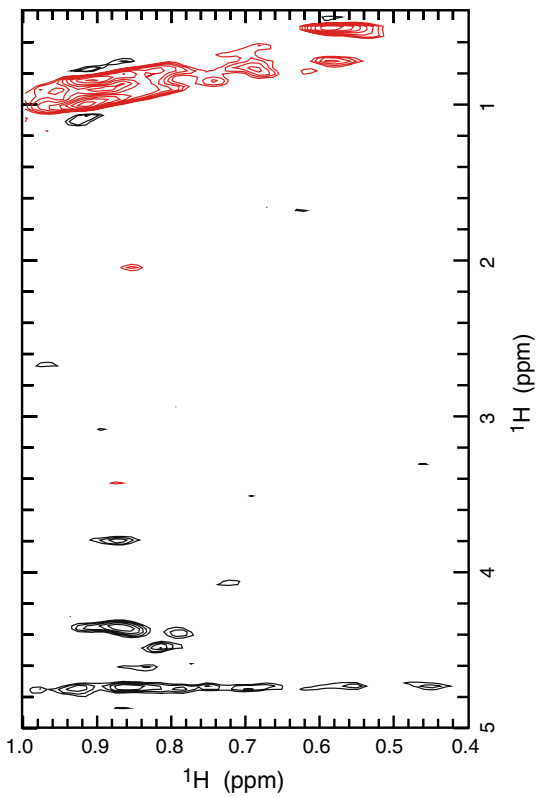

Fig. 10 NOESY-HSQC spectra for Vts1 SAM domain/TCE RNA complex. The spectrum was acquired using the pulse sequence of Fig. 7 by setting $t_2 = 0$. Filter parameters were identical as described for Fig. 9b. Other experimental details are given in the text

Theoretical optimization and analysis of the isotope filter pulse sequences are simplified by using average Hamiltonian theory to describe evolution of I-spin coherence under the heteronuclear scalar coupling Hamiltonian while an adiabatic sweep is applied to the S spin in an I_nS spin system. The compact results that emerge from average Hamiltonian theory in this context are likely to be applicable to other experimental NMR methods that utilize adiabatic sweeps in heteronuclear scalar-coupled spin systems.

The joint composite-rotation adiabatic-sweep isotope filter is extremely efficient in suppressing coherence from ^{1}H spins directly attached to ^{13}C nuclei. In all existing isotope filters, increased suppression efficiency inevitably is obtained at cost of increased filter length. Recently optimal control theory has been applied to the design of solution NMR pulse sequences for coherence transfer with optimal relaxation properties (Khaneja et al. 2004); similar methods may prove fruitful for further developments in J-filtration.

Acknowledgements This work was supported by NIH grants GM50291 (A.G. P.) and GM47021 (D. C.). E.R.V. acknowledges support from a National Science Foundation Graduate Research Fellowship. We thank Joel A. Butterwick (Columbia University), Thomas A. Edwards (Mt. Sinai School of Medicine), and Aneel K. Aggarwal (Mt. Sinai School of Medicine) for the Vts1 SAM domain/TCE 13mer RNA sample. Helpful discussions with Mark Rance (Univ. Cincinnati) are acknowledged gratefully.

References

Bennett AE, Gross JD, Wagner G (2003) Broadband ^{13}C-^{13}C adiabatic mixing in solution optimized for high fields. J Magn Reson 165:59–79

Breeze AL (2000) Isotope-filtered NMR methods for the study of biomolecular structure and interactions. Prog NMR Spectrosc 36:323–372

Böhlen J-M, Burghardt I, Rey M, Bodenhausen G (1990) Frequency-modulated "chirp" pulses for broadband inversion recovery in magnetic resonance. J Magn Reson 90:183–191

Edwards TA, Butterwick JA, Zeng L, Gupta YK, Wang X, Wharton RP, Palmer AG, Aggarwal AK (2006) Solution structure of the Vtsl SAM domain in the presence of RNA. J Mol Biol 356:1065–1072

Evans WAB, Powles JG (1967) Time-dependent Dyson expansion. Nuclear resonance signal in a rotating single crystal. Proc Phys Soc 92:1046–1054

Grzesiek S, Bax A (1993) Amino acid type determination in the sequential assignment procedure of uniformly $^{13}C/^{15}N$-enriched proteins. J Biomol NMR 3:185–204

Haeberlen U, Waugh JS (1968) Coherent averaging effects in magnetic resonance. Phys Rev 175:453–467

Hwang TL, Shaka AJ (1995) Water suppression that works. Excitation sculpting using arbitrary waveforms and pulsed field gradients. J Magn Reson Ser A 112:275–279

Kay LE, Keifer P, Saarinen T (1992) Pure absorption gradient enhanced heteronuclear single quantum correlation spectroscopy with improved sensitivity. J Am Chem Soc 114:10663–10665

Khaneja N, Li JS, Kehlet C, Luy B, Glaser SJ (2004) Broadband relaxation-optimized polarization transfer in magnetic resonance. Proc Natl Acad Sci USA 101:14742–14747

Kupče E, Freeman R (1995) Adiabatic pulses for wide-band inversion and broad-band decoupling. J Magn Reson Ser A 115:273–276

Kupče E, Freeman R (1997) Compensation for spin-spin coupling effects during adiabatic pulses. J Magn Reson 127:36–48

Levitt MH (1982) Symmetrical composite pulse sequences for NMR population inversion. I. Compensation of radiofrequency field inhomogeneity. J Magn Reson 48:234–264

Levitt MH (1986) Composite pulses. Prog NMR Spectrosc 18:61–122

Logan TM, Olejniczak ET, Xu RX, Fesik SW (1993) A general method for assigning NMR spectra of denatured proteins using 3D HC(CO)NH-TOCSY triple resonance experiments. J Biomol NMR 3:225–231

Marion D, Ikura M, Tschudin R, Bax A (1989) Rapid recording of 2D NMR spectra without phase cycling. Application to the study of hydrogen exchange in proteins. J Magn Reson 85:393–399

McCoy MA, Mueller L (1993) Selective decoupling. J Magn Reson Ser A 101:122–130

Mitschang L, Rinneberg H (2003) Broadband population inversion by a frequency-swept pulse beyond the adiabatic approximation. J Chem Phys 118:5496–5505

Otting G, Wüthrich K (1990) Heteronuclear filters in two-dimensional [^{1}H, ^{1}H] NMR spectroscopy: combined use with isotope labeling for studies of macromolecular conformation and intermolecular interactions. Q Rev Biophys 23:39–96

Palmer AG, Cavanagh J, Wright PE, Rance M (1991) Sensitivity improvement in proton-detected two-dimensional heteronuclear correlation NMR-spectroscopy. J Magn Reson 93:151–170

Peterson RD, Theimer CA, Wu HH, Feigon J (2004) New applications of 2D filtered/edited NOESY for assignment and structure elucidation of RNA and RNA-protein complexes. J Biomol NMR 28:59–67

Schleucher J, Schwendinger M, Sattler M, Schmidt P, Schedletzky O, Glaser SJ, Sørensen OW, Griesinger C (1994) A general enhancement scheme in heteronuclear multidimensional NMR employing pulsed field gradients. J Biomol NMR 4:301–306

Shaka AJ, Barker PB, Freeman R (1985) Computer-optimized decoupling scheme for wideband applications and low-level operation. J Magn Reson 64:547–552

Stuart AC, Borzilleri KA, Withka JM, Palmer AG (1999) Compensating for variations in ^{1}H-^{13}C scalar coupling constants in isotope-filtered NMR experiments. J Am Chem Soc 121:5346–5347

Tjandra N, Bax A (1997) Direct measurement of distances and angles in biomolecules by NMR in a dilute liquid crystalline medium. Science 278:1111–1114

Zwahlen C, Legault P, Vincent SJF, Greenblatt J, Konrat R, Kay LE (1997) Methods for measurement of intermolecular NOEs by multinuclear NMR spectroscopy: Application to a bacteriophage λ N-peptide/*boxB* RNA complex. J Am Chem Soc 119:6711–6721

Zwahlen C, Vincent SJF, Kay LE (1998) Analytical description of the effect of adiabatic pulses on IS, I_2S, and I_3S spin systems. J Magn Reson 130:169–175